RECENT RESULTS FROM AMY

Guinyun Kim

University of California

Davis, CA 95616, U.S.A.

and

KEK, Tsukuba 305, Japan

(Representing the AMY Collaboration)

ABSTRACT

Results from the AMY experiment at the TRISTAN e^+e^- collider are presented using a data sample of about 28 pb^{-1} at center of mass energies between 50 and 60.8 GeV. The measured value of R, which is about 2σ higher than the standard model expectation for c.m. energy above 56 GeV, is presented and several possible explanations are discussed. The results of the forward-backward asymmetry measurement of $e^+e^- \rightarrow b\bar{b}$ events, tests of QCD in the hadronic jets, and the search of heavy leptons are also presented.

Talk presented at KEK Topical Conference on e^+e^- Collision Physics
KEK, Tsukuba, Japan, May 17 - 19, 1989

1. Introduction

Results from the AMY experiment at the TRISTAN e^+e^- storage ring are presented using a data sample of about $28pb^{-1}$ at center of mass(c.m.) energies between 50 and 60.8 GeV . We measured the e^+e^- hadronic annihilation cross section and found it to be about 2σ higher than the standard model expectation for c.m. energies above 56 GeV. Several possible explanations for the high values of R are discussed. A measurement of the forward-backward charge asymmetry in the hadronic process, $e^+e^- \rightarrow b\bar{b}$, results from the study of hadronic jets, and the search for heavy leptons are also presented.

2. Measurements of R

We select multihadronic annihilation events by requiring five or more charged tracks with $|\cos\theta| \leq 0.85$ that originate from the interaction point, a total visible energy (E_{vis}) greater than half of the c.m. energy, a momentum imbalance along the beam direction with a magnitude less than $0.4E_{vis}$ and more than 3(5) GeV energy deposited in the barrel calorimeter at 50 and 52 (55 to 60.8) GeV. From the number of observed multihadron annihilation events (N_{ev}), we determine the R using the following relation

$$R = \frac{N_{ev} - N_{bkg}}{\epsilon(1+\delta)\int Ldt\sigma_{\mu\mu}(s)},$$

where N_{bkg} is the estimated number of background events remaining in the sample, ϵ is the detection efficiency for hadronic events determined from Monte Carlo (MC) simulations using the LUND 6.3 event generator,[1] $1+\delta$ is a correction factor for radiative effects calculated using the FKS program including full electro-weak radiative effects up to $O(\alpha^3)$,[2] $\int Ldt$ is the integrated luminosity and $\sigma_{\mu\mu}(s)$ is the lowest order QED cross section for $e^+e^- \rightarrow \mu^+\mu^-$ at the same c.m. energy. No correction is made for trigger efficiency since this is estimated by comparing redundant triggers to be better than 99.7%.

The overall normalization uncertainty contains energy independent systematic errors in the luminosity determination ($\sim$ 3.3%), the detection efficiency estimation ($\sim$ 1.3%), radiative corrections ($\sim$ 1.3%), event selection ($\sim$ 1.7%) and the background subtraction ($\sim$ 0.4%), which, when added in quadrature, result in a total normalization error of about 4.2 %.

The R measurements from the AMY are shown in Fig. 1a. The errors in the figure are calculated by combining in quadrature the point-to-point statistical errors and the overall normalization errors. The solid curve indicates the prediction of the five-quark standard model with M_Z=92GeV/c^2, $\sin^2\theta_W$=0.230 and $\Lambda_{\overline{MS}}$ =0.2 GeV. Also shown in the figure are the predictions of R in presence of a t quark or a fourth generation b′ quark at a mass of 24 GeV/c^2. The differences between measured and predicted values of R are also shown in Fig. 1b, together with the predictions for the cases of a t quark or a fourth generation b′ quark at full production. The measured values of R are higher than the standard model prediction above 56 GeV. The weighted average value of ΔR above 56 GeV is 0.47$\pm$0.23, about a 2σ effect.

If this effect is simply due to statistical fluctuation or systematic shift, then the same effect would not necessarily be observed by other groups. But, as you will hear from the TOPAZ and VENUS groups,[3] they also observe higher R values above $\sqrt{s}$=56 GeV. We consider possibilities that new particle productions are the cause for the higher R values. Candidates particles are: a) t quark; b) b′ quark; c) charged and neutral heavy leptons ($L^{\pm}$,L°); d) charged higgs ($H^{\pm}$); and e) spinless gauge boson (X°).

a) Pair production of t quarks

If the t quark pair is produced above 56 GeV, we expect ΔR to be of the order of 1.0, which is not consistent with our measurement. Moreover, since t quarks would be produced nearly at rest, the directions of decay products from one t quark would show little correlation with those from the other t quark, resulting in events with spherical shapes. The dimensionless variable Thrust[4]

(T) has been used to parameterize the event shape. It is 0.5 for events with an isotropic angular distribution of final state hadrons, and 1.0 for perfect back-to-back jets. Fig. 2-a shows the thrust distribution for the events at 60 GeV. Included in the figure are the expected distributions from a 5-flavor MC (shown as a dashed histogram) and that from a mixture of 90% 5-flavor and 10% t quark pair production (solid histogram). We select three regions of thrust; greater than 0.9, less than 0.8 and in between, and plot the fraction of events for each region for all c.m. energies in Fig. 2-b; the expectation from the 5-flavor MC is shown as a solid line.

The Thrust distribution of the data in Fig. 2-a is not consistent with the expectations for t quark production. In Fig. 2-b, the fraction of lower thrust (T<0.8) events is also consistent with the expectation from the 5-flavor MC. Therefore, the t quark can not account for the observed higher R values.

b) Pair production of b′ quarks

For the case of pair production of b′ quarks, ΔR is expected to be about 0.5, consistent with our measured results. If b′ quarks are produced, we expect the event shape to be different from that for ordinary multi-hadronic events. In order to select the events originating from b′ quarks, we have developed event selection cuts using MC simulated events. If the b′ quark decays via a charged current (CC) as in the case of the t quark, we expect spherical event shape, which is sometimes accompanied by an isolated lepton. However, Hou and Stuart[5] have recently pointed out that if b′ is lighter than t, the b′ quark would decay predominantly via one-loop-induced neutral currents (FCNC): $b' \rightarrow bg$, $b' \rightarrow bg^*$, and $b' \rightarrow b\gamma$. Since $b' \rightarrow bg$ (or $b\gamma$) is a two body decay, experimental signatures for these neutral current decays would differ from those of the charged current decay. Just above threshold, the events will be planar and pancake-like and, occasionally have an isolated photon with half of beam energy.

We have applied three separate event shapes, Thrust (T), Acoplanarity[6] (A), which reflects the extent to which the momentum vectors of the final state

hadrons from a common plane, and 'Lesser-Bi-Width'[7] (LBW) which is obtained by computing $(\sum P_T)_s/E_{vis}$, where $(\sum P_T)_s$ is the transverse momentum sum in each hemisphere divided by the plane normal to the thrust axis and taking a smaller value of the two. If we assume that all of 10% increase in R is due to the pair production of b′ quarks, we can estimate how many events are selected for various cuts using a sample MC simulated b′ events, In order to have good detection efficiency for pair produced b′ events, we use loose conditions for each variable; T<0.82, A>0.14, and LBW>0.17. We listed the number of events selected from data in Table 1, together with expectations from the 5-flavor MC and from a mixture of 90% 5-flavor and 10% pair production of b′ quark for both decay modes, normalized to the observed number of hadronic events at c.m. energies between 56 and 60.8 GeV. As shown in the table, the number of selected events are consistent with those expected from 5-flavor MC hadronic events and inconsistent with the MC estimate including b′. Therefore, a 10% increase in R due to b′ production is unlikely for both the CC and FCNC decay modes.

[Table 1] The number of events selected from data , 5-flavor MC hadrons(5F) and both decay modes of b′ MC

CUTS	5F (100%)	5F+CC (90%) (10%)	5F+FCNC (90%) (10%)	Data ($\sqrt{s}$=56-60.8)
T<.82	211	190+148=338	190+128=318	205
A>.14	157	141+110=251	141+110=251	162
LBW>.17	109	98+96=194	98+133=231	111

c) Pair production of charged or neutral heavy leptons ($L^{\pm}$, L°)

We consider here the possibility of a sequential fourth generation charged heavy leptons that decays to a massless neutrino and virtual W boson. In addition, we consider neutral heavy leptons that are massive and decay via mixing with light neutrinos. In both cases the expected increases in R are not enough

to explain the observed higher R values in our data. However, if we assume that a 10% increase in R is due to the pair production of charged or neutral heavy leptons, a number of events should pass the dedicated selection criteria[8] used in charged or neutral heavy lepton searches. The number of selected events are listed in Table 2, together with expectations from the 5-flavor M.C. and from a mixture of 90% 5-flavor MC and 10% charged or neutral heavy leptons, using the selection criteria for charged or neutral heavy leptons. All numbers are normalized to the observed number of hadronic events at c.m. energies between 56 and 60.8 GeV. The observed number of events are consistent with those expected from the 5-flavor MC. We can not attribute the excess events to the pair production of charged or neutral heavy leptons.

[Table 2] The number of events selected from charged (CHL) or neutral heavy lepton (NHL) selection cuts

CUTS	MC(5F) (100%)	MC(5F)+HL (90%) (10%)	Data ($\sqrt{s}$=56-60.8 GeV)
CHL selection	2.9	2 +129 =131	2
NHL selection	1.	1.+ 92=93	0

d) Pair production of charged Higgs ($H^{\pm}$)

Charged Higgs bosons, motivated by extended standard models or supersymmetry, are assumed to be produced via the reaction $e^+e^- \rightarrow H^+H^-$ with the cross section, $R_{H^+H^-} = 1/4\beta^3$. They are assumed to decay rapidly to the heaviest fermions possible, either heavy quarks or the heavy lepton τ and its neutrino. However, we studied only one decay process, $H^+ \rightarrow c\bar{s}$; here H^+H^- events would result in four-jets of hadrons.

Again, we have examined how many events identified as low thrust and four-jets would be observed in the data if higher R values were due to the pair production of charged Higgs. As shown in Table 3, the observed numbers in the

data are consistent with those expected in 5-flavor MC, and inconsistent with expectation from pair production of charged Higgs scalars.

[Table 3] The number of events with low thrust and 4-jets

CUTS	MC(5F) (100%)	MC(5F)+Higgs (90%) (10%)	Data ($\sqrt{s}$=56-60.8 GeV)
T<0.8 and 4-jets	19	17 + 52 =69	20

e) Spinless gauge boson (X°)

The spinless gauge boson was originally proposed to explain an excess of radiative Z° decay events at the CERN $p\bar{p}$ collider.[9] In some type of the composite models, the Z° is not elementary and the existence of a lighter spin zero partner X° is expected.[10] Thus, radiative transitions $Z^\circ \rightarrow X^\circ\gamma$ could conceivably take place, followed by subsequent decays of X° into lepton, quark or photon pairs. If the mass of the X° boson is within the energy range attainable with TRISTAN, we could observe the effects of X° to the processes[11] ; $e^+e^- \rightarrow l^+l^-, q\bar{q}$, and $\gamma\gamma$. In addition to the observed higher R values, AMY has also observed that the cross section for $e^+e^- \rightarrow \gamma\gamma$ is higher than the QED prediction for c.m. energies of 56 GeV and higher. This is shown in Fig. 3. The total cross sections for e^+e^-, $\gamma\gamma$, and $q\bar{q}$ were fitted to the corresponding electroweak predictions plus an additional X°-boson contribution allowing 4 free parameters: M_X, Γ_{ee}, Γ_{qq}, and $\Gamma_{\gamma\gamma}$. We get a best fit (χ^2=23.8 for 27 degrees of freedom) for $M_X = 58.2\text{GeV}/c^2$, $\Gamma_{ee} = 8.5 \times 10^{-5}$ GeV, Γ_{qq}=0.43GeV, and $\Gamma_{\gamma\gamma}$=1.2GeV. Results of the fit are shown in Fig. 4.

If this exciting possibility has any connection with reality, some effect might be seen in high energy $p\bar{p}$ collisions. Fig. 5 shows the distribution of the invariant mass of di-jet events from UA2.[12] In this figure, we can clearly see a bump due to the W and Z gauge boson. Our solution would add another bump around 58 GeV. It would be interesting to know what values of Γ_{qq} and $\Gamma_{\gamma\gamma}$ for a spinless

particle near 60 GeV can be ruled out by existing data from the CERN and TEVATRON $p\bar{p}$ colliders.

As discussed above, we find no simple explanation for the higher R values in terms of new particle production. We now examine the theoretical predictions for R from the standard model. In the standard model

$$R = 3\sum_q Q_q^2(1 + C_{EW}) \cdot (1 + C_{QCD}),$$

where C_{QCD} and C_{EW} are the QCD and electro-weak correction terms. At TRISTAN energies, these are about 5% and 25% respectively. Since the electro-weak correction term depends on M_Z and $\sin^2\theta_W$, the predicted values for R depend strongly on the mass of Z°. We determine the Z° mass by fitting the R measurements leaving M_Z and $\sin^2\theta_W$ as free parameters, fixing $\Lambda_{\overline{MS}}$ at 0.15GeV, using an error matrix method suggested by CELLO group.[47] Here, we have included in the fit previous measurements of R by VENUS and TOPAZ at 50 and 52 GeV[14] as well as those from PEP, PETRA, CESR and DORIS at lower energies.[15] Details of this analysis are described elsewhere.[16] We obtained $M_Z = 88.1^{+1.7}_{-1.5}\mathrm{GeV/c^2}$, and $\sin^2\theta_W = 0.238^{+0.031}_{-0.022}$ as plotted in Fig. 6, with the combined value from two direct production measurements of UA1 and UA2 groups at the CERN $p\bar{p}$ collider,[17] $M_Z = 91.9 \pm 1.8\mathrm{GeV/c^2}$, and $\sin^2\theta_W = 0.228 \pm 0.007$. The fitted results for M_Z are lower than those from direct production measurements. The new CDF measurement of the Z° mass, $M_Z = 90.4 \pm 1.9\mathrm{GeV/c^2}$, using the invariant mass of e^+e^- pairs,[18] presented at this conference, is also plotted in Fig. 6.

If M_Z is about 2 $\mathrm{GeV/c^2}$ lower than currently accepted value, what could we expect at SLC ? Fig. 7 shows the total cross sections for $e^+e^- \to Z^\circ \to \mu^+\mu^-$ as a function of $\sqrt{s} - M_Z$.[19] From this figure, we can see that the production rate at $\sqrt{s} - M_Z$=2 GeV is reduced to about half of the peak rate. If SLC runs at $\sqrt{s}$= 92 GeV and $M_Z = 88\mathrm{GeV/c^2}$, the production rate would be about 25% of the peak rate.

3. Forward-Backward Asymmetry for $e^+e^- \rightarrow b\bar{b}$

While there is still no direct evidence for the sixth quark (t quark), the scheme with three families of of lepton and quark doublets, including the t quark as a counterpart of the b quark, has been successful in explaining a wide range of experimental phenomena. It is therefore generally accepted that the t quark will eventually be found as higher energy accelerators become operational. Until then, it is important to check that the properties of the b quark are consistent with the interpretation of the b quark as a $T_3 = -1/2$ member of a $(t\ b)_L$ weak isospin doublet, where T_3 is the third component of weak isospin. The forward-backward asymmetry of the process $e^+e^- \rightarrow b\bar{b}$ is sensitive to T_3.

We extracted the forward-backward asymmetry of the $e^+e^- \rightarrow b\bar{b}$ process using 123 multihadronic inclusive muon events accumulated at c.m. energies between 52 and 57 GeV.[20] The inclusive muon events are selected from the multihadronic annihilation events by requiring the presence of at least one muon hit in an event. The details of the muon identification have been described previously.[21] The overall detection efficiency for muons above 3 GeV/c in the angular region of $|\cos\theta| \leq 0.74$ is 82%.

Backgrounds to the muon signal (hadron fakes) arise principally from hadrons formed from u, d, s, c, and b quarks, either from hadron showers in the hadron filter, where the debris reaches the muon chamber (punchthroughs), or by mesons that decay, before interacting in the hadron filter, to a muon that reaches the muon chamber (decay).

For the determination of the forward-backward asymmetry for $e^+e^- \rightarrow b\bar{b}$, we assume that the decays of c and b quarks to muons is known. This is justified because these quantities depend only on the decay kinematics of the parent quark and not on the dynamics of the $q\bar{q}$ pair production. We used the Lund 6.3 MC to estimate the distributions in transverse momentum relative to the Thrust axis for $c\bar{c}$, $b\bar{b}$, hadron fakes, and $b\bar{b}$ cascade decays. The muons from the semileptonic

decays of b flavor hadrons tend to have larger P_T values, reflecting the fact that b-flavored hadrons are heavier than those of other flavors. The cascade decay produces muons with charge opposite to those produced by direct decay, and thus contributes oppositely to the asymmetry. The MC study indicates that we can maximize the fraction of b quarks by only using events with muons with P_T greater than 0.7 GeV/c.

We extracted the forward-backward asymmetry after subtracting the effect of backgrounds estimated from the Monte Carlo study. We fitted the angular distribution, in the region of $|\cos\theta| \leq 0.6$, to the standard model expectation for $e^+e^- \to b\bar{b}$;

$$\frac{d\sigma}{d\cos\theta} = \frac{\pi\alpha^2}{2s} R_b (1 + \cos^2\theta + \frac{8}{3} A_b \cos\theta)$$

where α and s are the fine structure constant and the square of the c.m. energy, θ is defined as the angle of the outgoing b with respect to the incoming e^- direction, R_b is the ratio of the total cross section for $e^+e^- \to b\bar{b}$ to the QED result for mu-pair, and A_b is the forward-backward asymmetry. From the fitting $A_b = -0.72 \pm 0.31$ and $R_b = 0.57 \pm 0.19$ were obtained at an average c.m. energy of $\sqrt{s} = 55.2$ GeV, as shown in Fig. 8a, which are consistent with the standard model predictions of $A_b = -0.56$ and $R_b = 0.55$. Fig. 8b compares our result for A_b with those from previous measurements at lower energies.[22] In addition to the asymmetries for hadronic processes we showed those for leptonic processes[23] $e^+e^- \to \mu^+\mu^-$ and $e^+e^- \to \tau^+\tau^-$ in Fig. 9 together with those from previous measurements.[24] Overall agreement between the measurements and the standard model is good throughout the entire energy region explored so far. Thus, it confirms that the axial-vector coupling of the $b\bar{b}$ to the Z° is consistent with being $g_A^b = -1/2$. This in turn is consistent with the weak isospin asignment $T_{3L} = -1/2$ and $T_{3R} = 0$ for the b quark, therefore requiring the existence of the t quark.

4. Study of Hadronic Jets

Studies of the properties of jets produced in e^+e^- annihilations have provided much information regarding the nature of quarks and gluons and of the theory of their interactions, Quantum Chromodynamics (QCD).[25] We report the evidence for the non-Abelian nature of QCD and the properties of quark-induced and gluon-induced jets from measurements of multi-jet events.

In order to identify the jet multiplicity in the multi-hadronic event sample, we have adopted the jet clustering algorithm which was first employed by the JADE group.[26] In this algorithm, the minimum scaled invariant mass squared $y_{ij} = m_{ij}^2/E_{vis}^2$ where $m_{ij}^2 = 2E_iE_j(1-\cos\theta_{ij})$ is calculated for each pair of particles. If the smallest value of y_{ij} is smaller than a predetermined parameter, y_{cut}, they are combined into a cluster by summing the 4-momenta. This process is repeated using all combinations of clusters and remaining particles, until all of the y_{ij} values exceed y_{cut}. The number of clusters remaining at this stage is the jet multiplicity.

In Fig. 10, the values of the jet multiplicities as a function of y_{cut} from data are compared with the LUND 6.3 parton shower model[1] and the second order matrix element calculation of Gutbrod, Kramer and Schierholz (GKS)[27] which was used in LUND 6.2 MC.

4.1 Evidence for the Non-Abelian nature of QCD

Due to the non-Abelian nature of QCD, the gluons themselves carry color charge and, thus, couple to themselves. As a result, the QCD coupling strength, α_s, decreases with increasing Q^2 and the triple gluon vertex contributes to the production of four-jet events in e^+e^- annihilations.

We report here evidence for the non-Abelian nature of QCD from a study of multi-jet events observed at c.m. energies between 50 and 57 GeV. A comparison of the fraction of three-jet events with those from lower energy PETRA

experiments provides evidence for the Q^2 variation of α_s, while measurements of the angular distributions of four-jet events provide evidence for the triple gluon vertex.

In QCD, the fraction of three-jet events, R_3, is given by the relation[28]

$$R_3 = C_1(y_{min})\alpha_s + C_2(y_{min})\alpha_s^2$$

where y_{mim} is the minimum scaled parton-pair invariant mass which is similar to the parameter y_{cut} in the jet-cluster algorithm. Since the only Q^2 dependence is contained in α_s, with y_{min} fixed, the Q^2 dependence of R_3 reflects the Q^2 dependence of α_s.

The measured value of R_3 is affected by initial state radiation, event selection cuts, and detector acceptance. We have found that $y_{min} = y_{cut}$=0.08, where the correction to R_3 is negligible, from MC studies.[29] In Fig. 11, we plot the value of R_3 with y_{cut}=0.08 from AMY together with previousely published values at lower energies from JADE[28] and TASSO[30] as a function of E^2_{CM}. Over this range, the measured values of R_3 decrease with increasing Q^2. The χ^2 for a fit to constant α_s is 23.3 for 6 degrees of freedom. The χ^2 for a fit to a second order calculation of Kramer and Lampe[31] with $Q^2 = E^2_{CM}$, shown in the figure, is 6.1 for 6 degrees of freedom.

A further manifestation of colored gluons is the contribution of the triple-gluon vertex, corresponding to the diagram shown in Fig. 12a, to the production of four-jet events. In QCD, the dominant contribution, corresponding to 66% of the total, to the four-jet cross section is from the triple-gluon vertex corresponding to the diagram in Fig. 12a, with the diagram in Fig. 12b contributing only 4%. In the Abelian model, the diagram in Fig. 11a is forbidden while the diagram in Fig. 12b contributes 51%. The remaining second order process contributing to four-jet production is double gluon bremsstrahlung, shown in the diagrams in Fig. 12c, and is common to both models.

Bremsstrahlung gluons are polarized in the $q\bar{q}g$ plane.[32] When these gluons couple to two quarks, as in Fig. 12b, the direction of the quarks tends to be perpendicular to the direction of this polarization.[33] On the other hand, when the coupling is to a pair of gluons as in Fig. 12a, the two gluons have a slight preference for being along the line of the polarization.

In order to see this effect, we look at two kinds of angle distributions for four jet-events,[34] one is the angle between the plane defined by the two highest energy jets and that defined by the two lowest energy ones, θ_{BZ}, and the other is the angle between the vector difference of the momentum of the two highest energy jets and that of the two lowest energy jets, θ^*_{NR}. Fig. 13a and 13b shows the distribution of θ_{BZ} and $|\cos\theta^*_{NR}|$, respectively, for the data and for the MC prediction for both QCD and the Abelian model. In both cases, the LUND 6.2 MC with the second order Calculation of GKS[27] was used to generate the events. In both distributions, the data show a clear preference for QCD.

4.2 The properties of Quark and Gluon jets

In QCD, gluons have a color factor that is larger than that of quarks by a factor of 9/4, leading one to expect gluon jets to differ from quark jets of the same energy.[35] In particular, the higher color factor should result in gluons radiating more soft gluons and thus fragmenting into more particles than quarks, resulting in softer and fatter jets.[33] We report on an experimental comparison of the characteristics of quark-induced and gluon-induced jets based on an analysis of three-jet events selected from hadronic events observed at c.m. energies between 50 and 60.8 GeV.[36]

The jets are ordered according to the angles between jets: jet 1 is defined as the jet opposite to the two jets that have the smallest opening angle, jet 3 is opposite to those with the largest opening angle. Since gluon radiation is a brehmstrahlung-like process, the gluon is typically emitted close to one of the quarks and is usually the lowest energy parton in the final state. Thus, it

is expected that the jet 3 sample will be gluon enriched relative to the jet 1 and jet 2 samples, which are expected to be quark enriched. We determine the "calculated" energy of each jet, E_{cal}^{jet}, by using energy-momentum conservation and the opening angles between the three jets.

Two different QCD-motivated MC event generators were used to study the effectiveness of our selection procedures: the LUND 6.2 matrix element model[37] with the independent fragmentation scheme of Hoyer et al.,[38] and the LUND 6.3 parton shower model with string fragmentation [1]. The LUND 6.2 matrix element calculation uses terms up to second order in the QCD coupling strength, α_s. In the LUND 6.3 parton shower calculation, the partons are made to branch into other partons of less virtuality via a recursive scheme using a leading logarithm approximation (LLA). The results indicate that for visible jet energies in the range $10 \leq E_{vis}^{jet} \leq 16$ GeV, approximately two-thirds of the jet 3 sample corresponds to gluon-induced jets.

Since in our jet identification procedure the gluon-enriched jet sample corresponds to the jets with the lowest value of E_{cal}^{jet} in each event, there is little energy overlap with jets in the quark-enriched sample. Thus, comparisons are best done using variables that have little variation with E_{cal}^{jet}. Also, since the particle-jet correspondence is most reliable for the higher energy particles in a jet, we chose variables that are dominated by the leading particles in the jet. Specifically, we use the rapidity relative to the jet axis of the most energetic particle (leading particle) in each jet ($\eta = \frac{1}{2}\ln\frac{E+p_\parallel}{E-p_\parallel}$, where E is the leading particle's energy and $p_\parallel$ is its momentum component parallel to the jet direction), and the fraction of E_{vis}^{jet} that is contained in a cone of half angle $\frac{60^\circ}{\sqrt{E_{vis}^{jet}}}$ that is coaxial with the jet direction (ξ). (The $\sqrt{E_{vis}^{jet}}$ denominator is motivated by the expectation that the widths of hadron jets decrease with the jet energy.[39])

In Figs. 14a and 14b, we show the distributions of the mean values of η and ξ as a function of the visible jet energy (E_{vis}^{jet}) for the quark-enriched and gluon-enriched jet samples. The figures indicate that that the leading particles in the

quark-enriched jet sample tend to have a higher rapidity than its counterpart in the gluon-enriched jet sample and that the energy in quark-enriched jets is more concentrated in the core of the jet. In both cases, the behavior is not strongly dependent on the energy of the jet.

For a more detailed comparison, we compare the quark and gluon jets that have the same E_{vis}^{jet}, in the range between 13 and 16 GeV, the highest visible energy range where there are a reasonable number of jets in the jet 3 sample. In Fig. 15a (15b) we show the distributions of η for the quark- (gluon-)enriched jets. The η distribution for the gluon-enriched jet sample is clearly different from that for the quark-enriched jets. As a check that the observed difference between quark and gluon jets is not an artifact of our jet clustering and identification procedure, we performed the same analysis on simulated events that were generated using the matrix element generator with independent fragmentation, where gluons and quarks are made to fragment in the same way. The results of this simulation for jets 1 and 2 (jet 3) are shown in Fig. 15a (15b) as the dashed histogram. The independent fragmentation model gives reasonable agreement with the observed distributions for the quark-enriched jets. As expected, the model predicts the η distribution for jet 3 to be similar to that for jets 1 and 2, in disagreement with our observations. This indicates that the differences observed in the data reflect genuine differences in the fragmentation process for the two jet samples. The results of the LLA model, shown as dotted lines in the figures, show a different behaviour for quarks and gluons, reproducing the measured distributions reasonably well.

Fig. 16a (16b) shows the distributions of ξ for the quark- (gluon-)enriched jet samples for E_{vis}^{jet} between 13 and 16 GeV. The quark-enriched sample shows a peaking towards 100% while the distribution for the gluon-enriched sample is much broader; many of the jets having little or none of its energy in the core. The dashed histogram in both figures shows the results of the same analysis on the simulated independently fragmented events, which clearly disagrees with our measurements for the gluon-enriched sample. The LLA model (dotted line)

shows better agreement with the data.

5. Search for New Heavy Leptons

We report results from searches for new heavy leptons at the c.m. energies between 50 and 60.8 GeV. The search is based on the analysis of event shape and the lepton identification in the events. Both charged and neutral heavy leptons are considered. These analyses are also applicable to searches for leptoquarks and colored leptons.

5.1 Search for Charged Heavy Leptons ($L^{\pm}$)

We have searched for charged heavy fourth-generation lepton, allowing for the possibility that the associated neutrino (L°) is massive but stable. A pair of charged heavy leptons is produced via $e^+e^- \rightarrow L^+L^-$ with cross section $\sigma = \sigma_{\mu\mu}\beta(3-\beta^2)/2$, where β=v/c, and v is the velocity of the charged heavy lepton.

When δ, the mass difference between $L^{\pm}$ and L°, is greater than pion mass, charged heavy lepton decays into its own neutrino and any of the lower mass lepton or quark doublets. From lepton universality and quark flavor independence, we expect the probabilities for decay to each fermion doublet (3 leptons and 2×3 colored quarks) to be equal with branching ratios of one-ninth for decays to each of the three known lepton doublets, and a branching ratio of two-thirds for decays into hadrons. The experimental signatures, we have searched for, are: (i) acoplanar jets with large missing energy momentum due to two or three missing neutrinos (hadronic mode, corresponding to 8/9 of the decays); and (ii) acoplanar jets, an isolated electron or muon and large missing energy momentum due to three missing neutrinos (lepton-hadron mode, corresponding to 8/27 of the deacys). Details of this analysis are described eleswhere.[8]

The detection efficiency for the hadronic mode (the lepton-hadron mode), in the massless neutrino case, ranges from 20% (10%) for $\beta < 0.3$ to 4% (2%) at

β=0.8. The efficiency does not depend strongly on the assumed neutrino mass up to δ of about 7GeV/c^2, and rapidly drops for smaller δ. 3 (3) events survive the hadronic (lepton-hadron) mode selection cuts, while about 4 (2) are expected from the background processes at the c.m. energies between 50 to 60.5(57) GeV.

The 95% CL excluded region in the charged heavy lepton mass and neutrino mass plane is shown in Fig. 17. It has been extracted using the $\beta(3-\beta^2)/2$ threshold factor, corrected for the effects of initial state radiation.[40] The region excluded by the lepton-hadron mode analysis is contained entirely within the region excluded by the hadronic mode. Nevertheless, the combination of the two modes makes our limits insensitive to the uncertainty of decay branching fractions.

If δ is less than pion mass, the charged heavy lepton would be stable. The experimental signature for pair production of stable charged heavy leptons is an excess of collinear two charged particle events. For charged heavy lepton masses for $\beta \leq 0.614$, the lepton penetrates the magnet iron and passes the muon identification criteria. If the charged heavy lepton mass corresponds to a $\beta < 0.65$, they do not penetrate the iron yoke, and are identified as neither muons nor electrons. We have looked for the excesses from the mu-pair events and collinear non-mu and non-electron charged pair events. Combining both searches, a 95% CL lower mass limit of 30.1 GeV/c^2 is set. The excluded region for stable charged heavy leptons is also indicated in Fig.17. Also shown are the results from previous experiments.[41]

5.2 Search for Neutral Heavy Leptons (L°)

In the search for charged heavy leptons, the associated neutrino was assumed to be stable, even in the case where it was considered to be massive. Here we assume the massive neutrino (L°: neutral heavy lepton) is unstable and lighter than its charged partner; we examine both the possibilty of Dirac- or Majorana-type neutrinos.

Neutral heavy leptons can be pair produced through s-channel annihilation via the Z°, with the cross section:

$$\sigma = \sigma_{\nu\bar{\nu}} \times T(\beta).$$

Here $\sigma_{\nu\bar{\nu}}$ is the cross section for massless neutrino pair production and the threshold factor $T(\beta) = \beta(3+\beta^3)/4$ for Dirac L° and $T(\beta) = \beta^3$ for Majorana L°. There is more suppression near threshold for Majorana L° compared to Dirac L°, and the cross sections become the same at high energy. There are two kinds of decay models for neutral heavy leptons: one is the L° decays via the weak charged current (CC) through a virtual W, assuming that L° mixes with one of the known lepton doublets, and the other is via the flavor-changing neutral current (FCNC) through a virtual Z°.

Here we report on searches for CC decay mode of L° for both Dirac and Majorana cases and for FCNC decay mode of L° for Dirac case.

a) Charged Current decay mode of L°

Since neutral heavy leptons are expected to decay into a lepton plus hadrons with a branching ratio of 2/3, we consider the case where at least one of the W's decays hadronically, which should occur approximately 8/9 of the time. Such event are expected to have the following signatures: (i) at least two leptons (e or μ) should appear in the event; (ii) the leptons tend to be isolated from other particles and have rather high momentum; (iii) since the search is confined to rather massive neutrinos, the event shape should be rather spherical.

To ensure high trigger and track reconstruction efficiencies, the search is restricted to L°s decaying within 5cm of the interaction point. This places a lower limit on the sensitivity to the mixing level. We also assume mixing with the tau-neutrino is small compared with electron or muon neutrino so that neutral heavy lepton decays to either electrons or muons with hadrons. Details of this analysis are described eleswhere.[8,42]

In order to obtain the limits we assume that the L_s^o are short lived ($c\gamma\beta\tau_{L^o} \rightarrow 0$), so that all decays are within 5cm of the interaction point, excluded regions of $8.2 \leq M_{L^o_{Dirac}} \leq 26.5$ GeV/c^2 and $8.3 \leq M_{L^o_{Majorana}} \leq 22.4$ GeV/c^2 at 95% C.L. for mixing to electron neutrinos are obtained. Corresponding limits for mixing to muon neutrinos are $7.8 \leq M_{L^o_{Dirac}} \leq 28.1$ GeV/c^2 and $8.1 \leq M_{L^o_{Majorana}} \leq 24.9$ GeV/c^2. Limits for equal mixing are $8.0 \leq M_{L^o_{Dirac}} \leq 27.2$ GeV/c^2 and $8.1 \leq M_{L^o_{Majorana}} \leq 23.6$ GeV/c^2.

Taking into account the probability for both L_s^o to decay within 5cm of the interaction point, we obtain limits on the mixing parameter $|U_{\ell L}|^2$ vs M_{L^o}. Mixing to electron and muon neutrinos excluded regions at 95% C.L. for L^o_{Dirac} are shown in Fig. 18a. Corresponding limits for $L^o_{Majorana}$ are shown in Fig. 18b. Limits on $(|U_{eL}|^2 + |U_{\mu L}|^2)$ vs M_{L^o} for equal mixing ($|U_{eL}|^2 = |U_{\mu L}|^2$) are shown in Fig. 18c.

b) Flavor Changing Neutral Current decay mode of L°

Since, in this case, the neutral heavy lepton decays into a neutrino and a virtual Z°, at least two neutrinos are included in the final states. The expected event signatures are (i) two acoplanar jets with large missing energy momentum ($\sim$ 50%) and (ii) mono-jet events ($\sim$ 30%). We searched for mono-jet events, which were originally suggested to explain the unusall mono-jet events observed at CERN $p\bar{p}$ collider.[43]

In order to select mono-jet events, the following selection criteria have been developed: (1) at least five charged tracks with $|\cos\theta| \leq 0.85$ and more than 3 GeV energy deposited in the barrel calorimeter; (2) $0.25 \leq E_{vis}/\sqrt{s} \leq 0.65$; (3) the polar angle of thrust axis satisfies $|\cos\theta_T| \leq 0.7$; (4) the total transverse momentum of the event is greater than $0.2\sqrt{s}$; (5) one hemisphere defined by the plane normal to the thrust axis must contain energy deposition less than $0.05E_{vis}$; (6) No more than $0.125\sqrt{s}$ of energy deposited in the endcap calorimeters.

The selection efficiency for L° pair production is maximum at $M_{L^o} = 15$GeV/c^2 (10.4% with mono-jet branching fractions). The efficiency decreases to 2.3% at

$M_{L^\circ} = 25 GeV/c^2$ and 7.1% at $M_{L^\circ} = 5 GeV/c^2$. No candidate events survive the selection at c.m. energies between 50 and 60.8 GeV. We obtain the 95% C.L. excluded mass region, 6.9 $GeV/c^2 \leq M_{L^\circ} \leq 20.1 GeV/c^2$, which extends previously obtained limits by MAC.[44]

5.3 Search for Leptoquarks and Colored Leptons

a) Leptoquarks

Leptoquarks that couple to lepton-quark pairs arise in various theoretical models such as technicolor[45] and composite schemes.[46] Here, we consider only second generation leptoquarks of charge 2/3 and spin zero based on the specific model by B. and F. Schrempp.[45] Since generation quantum number is conserved in this model, a second generation leptoquark χ_μ can only decay into either $c\bar{\nu}_\mu$ or $s\mu^+$.

The differential cross section for pair production of charged color triplet spinless bosons in e^+e^- annihilation is proportional to $3Q^2\beta^3 \sin^2\theta$, where β is the c.m. velocity of the χ_μ, m_{χ_μ} is the leptoquark mass, Q=2/3 and θ is the production angle with respect to the beam direction.

The distinctive event topologies for leptoquark pair production are clasified into three: 1) two acoplanar jets with large missing energy momentum ($e^+e^- \rightarrow \chi_\mu \bar{\chi}_\mu \rightarrow c\bar{\nu}_\mu \bar{c}\nu_\mu$); 2) two jets with an isolated muon and missing momentum ($e^+e^- \rightarrow \chi_\mu \bar{\chi}_\mu \rightarrow c\bar{\nu}_\mu \bar{s}\mu^-$ or $\bar{c}\nu_\mu s\mu^+$); 3) two jets with two isolated muons ($e^+e^- \rightarrow \chi_\mu \bar{\chi}_\mu \rightarrow s\mu^+ \bar{s}\mu^-$).

Events of class 1) and 2) are similar to the signatures of hadronic mode and lepton-hadron modes of charged heavy lepton pair production, respectively. The experimental signature of class 3) is similar to that of neutral heavy leptons mixing with the muon generation. Therefore, we just applied the selection cuts for charged and neutral heavy leptons to leptoquarks. The detection efficiencies for 1), 2) and 3) classes at β=0.745 are 21.1, 24.5 and 47.9 %, respectively

The 95% C.L. mass limits for leptoquarks, obtained as a function of mass and branching ratio $\chi_\mu \rightarrow c\bar{\nu}_\mu$, are shown in Fig. 19. Also shown are previous results from PETRA.[47]

b) Colored Leptons

In some composite models,[48] color octet leptons l_8 are introduced and expected to be produced at present accelerators. They decay into a gluon and their color singlet partner, the ordinary lepton. The total cross secton for the pair production of colored leptons is

$$\sigma_{l_8} = 8 \cdot F(q^2) \cdot \sigma_l$$

where 8 is the color factor, and $F(q^2)$ is form factor to account for the compositeness of these objects; σ_l is the cross section for the production of ordinary leptons.

Considered here are the pair production of colored neutrios (ν_8) and colored muons (μ_8). The signatures of colored neutrino pairs are acoplanar jets with large missing energy momentum, and those of colored muon pairs are two μ and two-jet events.

If we neglect the differences in quark and gluon fragmentation and assume the lifetime of colored leptons is short enough so that they decay promptly at the interaction point, the topologies of $\nu_8\bar{\nu}_8$ and $\mu_8\bar{\mu}_8$ events are the same as those of classes 1) ($c\bar{\nu}_\mu\ \bar{c}\nu_\mu$) and 3) ($s\mu^+\ \bar{s}\mu^-$) for leptoquark pair events. Therefore, limits on ν_8 and μ_8 productions can be set using the selection efficiencies of classes 1) and 3) for the leptoquark pair events described in previous section. The resulting 95% C.L. limits for the form factors and masses are shown in Fig. 20 together with previous results.[47]

6. Conclusion

We have measured the e^+e^- hadronic annihilation cross section at the c.m. energies from 50 to 60.8 GeV and found to be about 2σ higher than the S.M. expectation for c.m. energies above 56 GeV. We could not find any simple explanations for this in terms of the pair production of several new particles. Our measured total cross sections for Bhabha, $\gamma\gamma$ and hadrons(R) were well fitted to the corresponding predictions with S.M. and an additional spinless gauge boson with mass $M_X = 58.2\text{GeV}/c^2$ (χ^2=23.8 for 27 degrees of freedom). The higher R values are also accomodated in the S.M. if the Z^0 mass is lower than currently accepted value. We have measured a $b\bar{b}$ charge asymmetry using inclusive muon events and found it to be consistent with the S.M. predictions, implying the existence of the t quark. We have observed the evidence of non-Abelian natures of QCD and a difference between quark and gluon jets. No new heavy leptons have been observed up to $\sqrt{s}$=60.8 GeV.

I thank the TRISTAN staff for the rapid commisioning and excellent operation of the storage ring. In addition I acknowledge the strong support and enthusiastic assistance provided by the staffs of the AMY home institutions. I would like to thank my AMY colleagues for this opportunity to present our results. This work has been supported by the Japan Ministry of Education, Science and Culture (Monbusho), the U.S. Department of Energy and National Science Foundation, the Korean Science and Engineering Foundation and Ministry of Education, and the Academia Sinica of the People's Republic of China.

REFERENCES

1) T. Sjostrand and M. Bengtsson, Comput. Phys. Commun. **43**, 367 (1987); M.Bengtsson and T.Sjostrand, Phys. Lett. **185B**, 435 (1987).

2) J. Fujimoto and Y. Shimizu, Mod. Phys. Lett. **A3**, 581 (1988); J.Fujimoto, K.Kato and Y.Shimuizu, Prog. Theor. Phys. **79**, 701 (1988).

3) S. Suzuki(TOPAZ), Talk in this conference;
K. Ogawa(VENUS), Talk in this conference.

4) E. Fahri, Phys. Rev. Lett., **39**, 1587 (1977).

5) Wei-Shu Hou and R.G.Stuart, Phys. Rev. Lett. **62**, 617 (1989)

6) A.De Rujula, Nucl. Phys. **B 318**, 387 (1978).

7) S. Eno *et al.*(AMY), Submitted to Phys. Rev. Lett.

8) G.N.Kim *et al.*(AMY), Phys. Rev. Lett. **61**, 911 (1988);
G.N.Kim *et al.*(AMY), KEK Preprint 88-42.

9) G. Arnison *et al.*(UA1), Phys. Lett. **135B**, 250 (1984);
P. Bagnaia *et al.*(UA2), Phys. Lett. **129B**, 130 (1983).

10) L. Abbot and E. Farhi, Phys. Lett. **101B**, 69 (1981);
H. Harari and N. Seiberg, Phys. Lett. **98B**, 269 (1981);
R.D. Peccei, Phys. Lett. **136B**, 121 (1984);
M.J. Puncan and M. Veltman, Phys. Lett. **139B**, 310 (1984).

11) W. Hollik, F. Schrempp and B. Schrempp, Phys. Lett. **140B**, 424 (1984); F. Bopp, S. Brandt, H. Dahmen, D. Schiller and D. Wahner, Z. Phys. **C24**, 367 (1984).

12) J.P. Repellin, in *Proceedings of the 7th International Conference on Physics in Collision, Tsukuba, 1987,* edited by T. Kondo and K. Takahashi (World Scientific, Teaneck, NJ 07666, USA, 1988) p. 235.

13) H.J.Behrend *et al.*(CELLO), Phys. Lett. **183B**, 400 (1987).

14) M.Yamauchi, KEK Preprint KEK 88-63.

15) E.Fernandez *et al.*(MAC) Phys. Rev. **D 31**, 1537 (1983);
D.Bender *et al.*(HRS), Phys. Rev. **D 31**, 1 (1983);
R. Brandelik *et al.*(TASSO), Phys. Lett. **113B**, 499 (1982);
B. Adeva *et al.*(MARK-J), Phys. Rev. Lett, **50**, 799 (1983);
W. Bartel *et al.*(JADE), Phys. Lett. **129B**, 145 (1983);
L.Criegee and G.Knies (PLUTO), Phys. Rep. **83**, 153 (1982).

16) T. Mori *et al.*(AMY), Phys. Lett. **218B**, 499 (1989).

17) U.Amaldi *et al.*, Phys. Rev. **D 36**, 1385 (1987).

18) L.Gladney, Talk in this Conference.

19) R. Klesiss, in CERN 86-02, Vol. 1, p.153.

20) H.Sagawa *et al.*(AMY), Submitted to Phys. Rev. Lett.

21) S.Igarashi, *et al.*(AMY), Phys. Rev. Lett. **60**, 2359 (1988).

22) W.Bartel *et al.*(JADE), Phys. Lett. **146B**, 437 (1984);
M.Althoff *et al.*(TASSO), Phys. Lett. **146B**, 443 (1984);
H.J.Behrend *et al.*(CELLO), Z. Phys. **C19**, 291 (1983);
B.Adeva *et al.*(MARK J), Phys. Rev. Lett. **51**, 43 (1983);
C.R.Ng *et al.*(HRS), ANL-HEP-PR-88-11;
H.R.Band *et al.*(MAC), Phys. Lett. **218B**, 369 (1989).

23) A. Bacala *et al.*(AMY), Phys. Lett. **218B**, 112 (1989).

24) M. Derrick *et al.* (HRS), Phys. Rev. **D 31**, 2352 (1985);
W. Ash *et al.* (MAC), Phys. Rev. Lett. **55**, 1831 (1985);
M.E. Levi *et al.* (MARK-II), Phys. Rev. Lett. **51**, 1941 (1983);
B. Adeva *et al.* (MARK-J), Phys. Rev. Lett. **55**, 665 (1985);
W. Bartel *et al.* (JADE), Z. Phys. **C 26**, 507 (1985);
Ch. Berger *et al.* (PLUTO), Z. Phys. **C 27**, 341 (1985);
H.J. Behrend *et al.* (CELLO), DESY Preprint 87-005;
M. Althoff *et al.* (TASSO), Z. Phys. **C 22**, 13 (1984).

25) H. Fritzsch, M. Gell-Mann and H. Leutwyler, Phys. Lett. **47B**, 365 (1973); D.J. Gross and F. Wilczek, Phys. Rev. Lett. **30**, 1343 (1973); H.D. Politzer, Phys. Rev. Lett. **30**, 1346 (1973).

26) W. Bartel *et al.* (JADE), Z. Phys. **C 33**, 23 (1986).

27) F. Gutbrod, G. Kramer, and G. Schierholz, Z. Phys. **C 11**, 315 (1982).

28) S. Bethke *et al.* (JADE), Phys. Lett. **213B**, 235 (1988).

29) I.H. Park *et al.* (AMY), Phys. Rev. Lett. **62** , 1713 (1989).

30) W. Braunschweig *et al.* (TASSO), DESY Preprint 88-046.

31) G. Kramer and K. Lampe, DESY Preprint 86-103; 86-119.

32) H. Olsen, P. Osland and I. Overbo, Phys. Lett. **89B**, 221 (1980).

33) S.J. Brodsky, T. DeGrand and R. Schwitters, Phys. Lett. **79b**, 1585 (1978).

34) M. Bengtsson and P.M. Zerwas, Phys. Lett. **20b**, 306 (1988);
M. Bengtsson, Aachen preprint PITHA 88/12 (1988).

35) J. Ellis and I. Karliner, Nucl. Phys. **B148**, 141 (1979).

36) Y.K. Kim *et al.*(AMY), Submitted to Phys. Rev. Lett.

37) T. Sjostrand, Comput. Phys. Commun. **39**, 347 (1986).

38) P. Hoyer *et al.*, Nucl. Phys. **B161**, 349 (1979).

39) Yu. L. Dokshitzer, V.A. Khoze and S.I. Troyan, DESY Preprint 80-093.

40) J. Fujimoto, K. Kato and Y. Shimimzu, KEK 87-69 (1987).We calculated the effects to be -17%, -25%, and -31% for heavy leptons with $\beta = 0.265$, 0.168, and 0.119, respectively.

41) R. Prepost, in *Proceedings of the 7th International Conference on Physics in Collision, Tsukuba, 1987,* edited by T. Kondo and K. Takahashi (World Scientific, Teaneck, NJ 07666, USA, 1988) p.107.

42) M. Shaw *et al.*(AMY), Submitted to Phys. Rev. Lett.

43) G. Arnison *et al.*(UA1), Phys. Lett. **139B**, 115 (1984)

44) W.W. Ash *et al.*(MAC), Phy. Rev. Lett. **54**, 2477 (1985).

45) J. Preskill, Nucl. Phys. **B177**, 21 (1981);
B. Schrempp and F. Schrempp, Phys. Lett. **153B**, 101 (1985).

46) R.N. Mohapatra, G. Segre, and L. Wolfenstein, Phys. Lett. **145B**, 433 (1985).

47) H.J. Behrend *et al.*(CELLO), Phys. Lett. **178B**, 452 (1986);
W. Bartel *et al.*(JADE), DESY Preprint 87-031 (1987).

48) S.F. King and S.R. Sharpe, Nucl. Phys. **B253**, 1 (1985);
H. Harari, Phys. Lett. **156B**, 250 (1985).

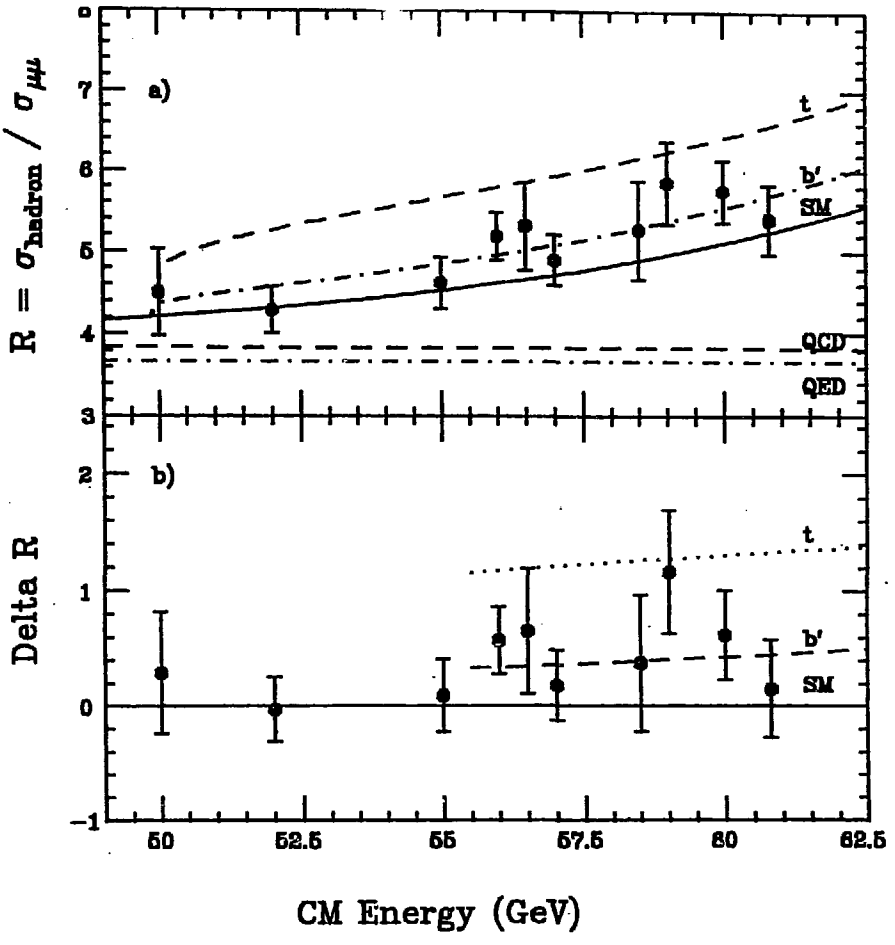

Figure 1. a) R measurements and b) ΔR

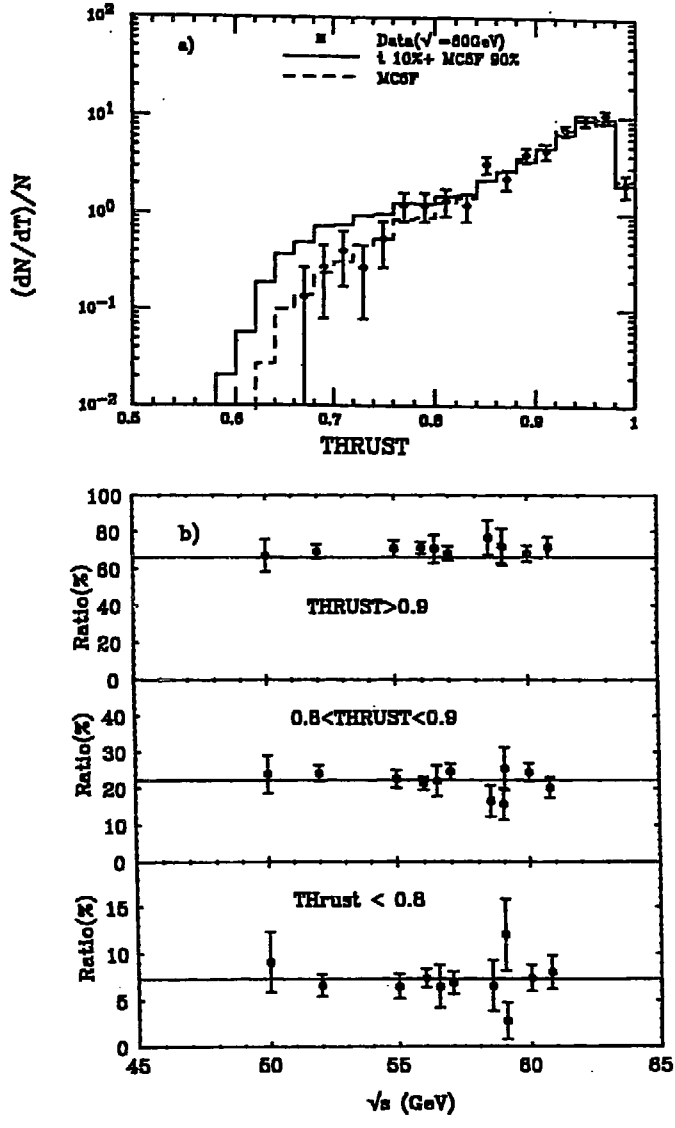

Figure 2. a) Thrust distribution. b) The fraction of events for each thrust region. The solid line indicate the expectation from 5-flavour hadronic MC events.

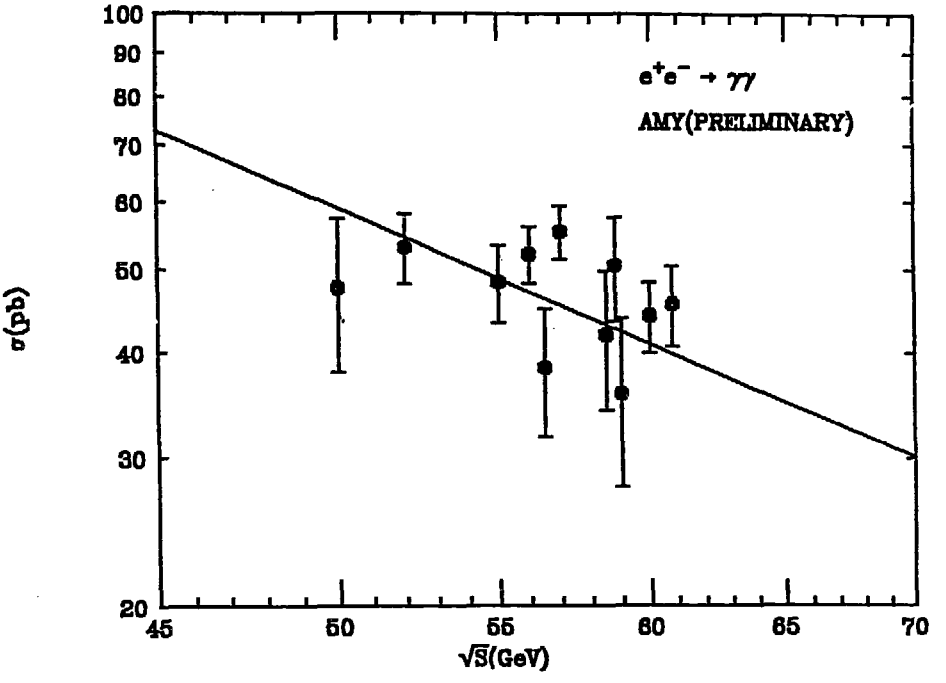

Figure 3. Total cross section for $e^+e^- \to \gamma\gamma$ as a function of c.m. energies. The solid line indicate the standard model prediction.

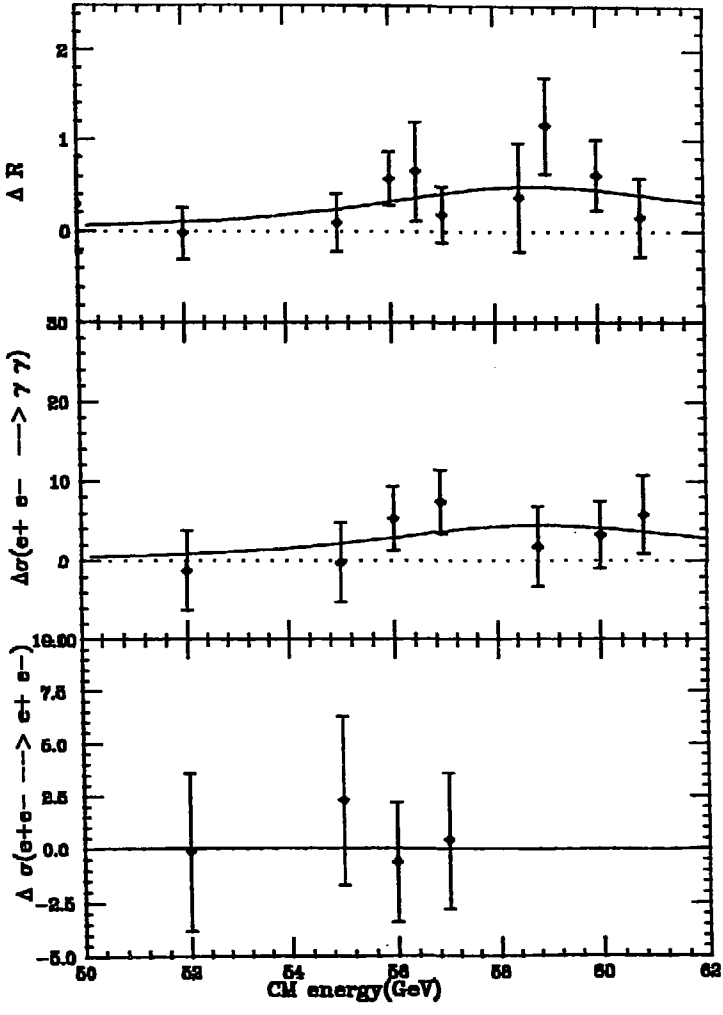

Figure 4. Results of the fit(solid line) for M_X=58.2GeV.

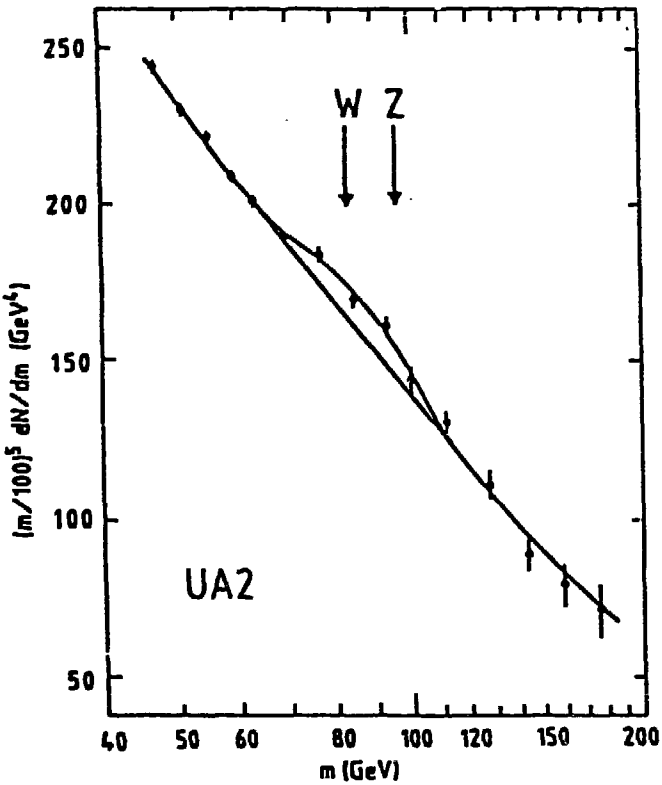

Figure 5. The invariant mass for dijet events from UA2

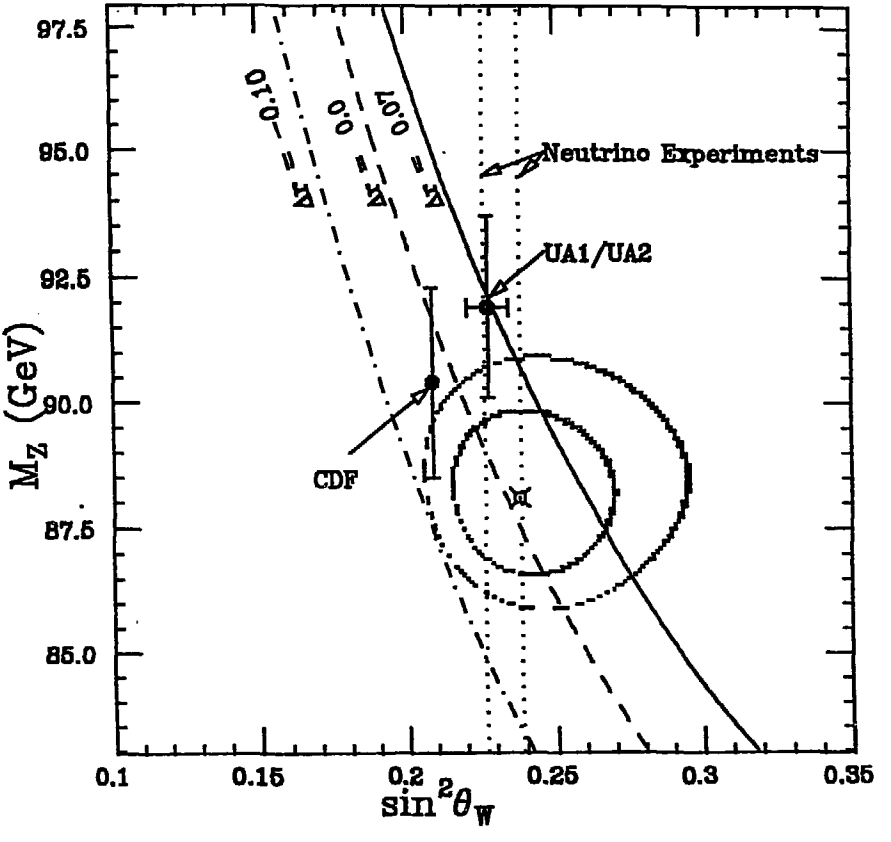

Figure 6. The results from the fitting for M_Z and $\sin^2\theta_W$. Also shown in the figure are the combined result of UA1 and UA2 , the recent result from CDF and one sigma band of $\sin^2\theta_W$ value from the neutrino experiments.

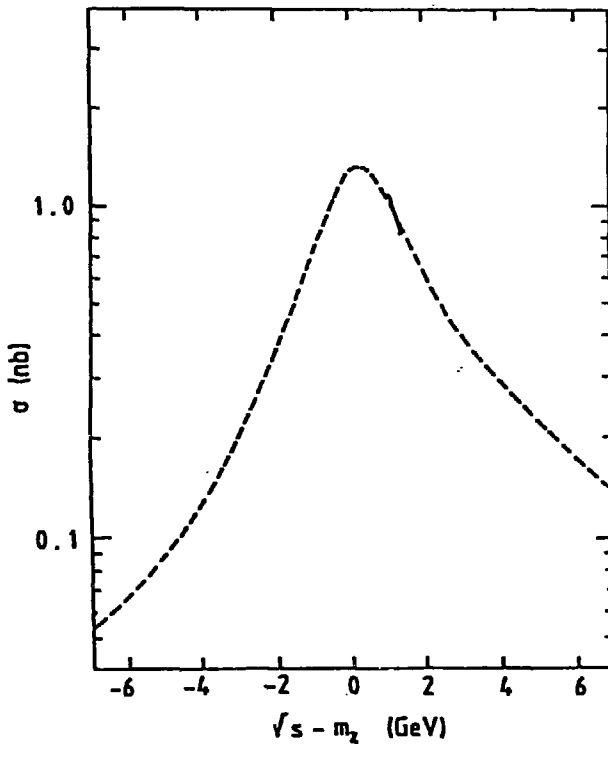

Figure 7. Total cross section for $e^+e^- \rightarrow Z^o \rightarrow \mu^+\mu^-$ as a function of energy for M_Z=90GeV, which are founded in reference 19.

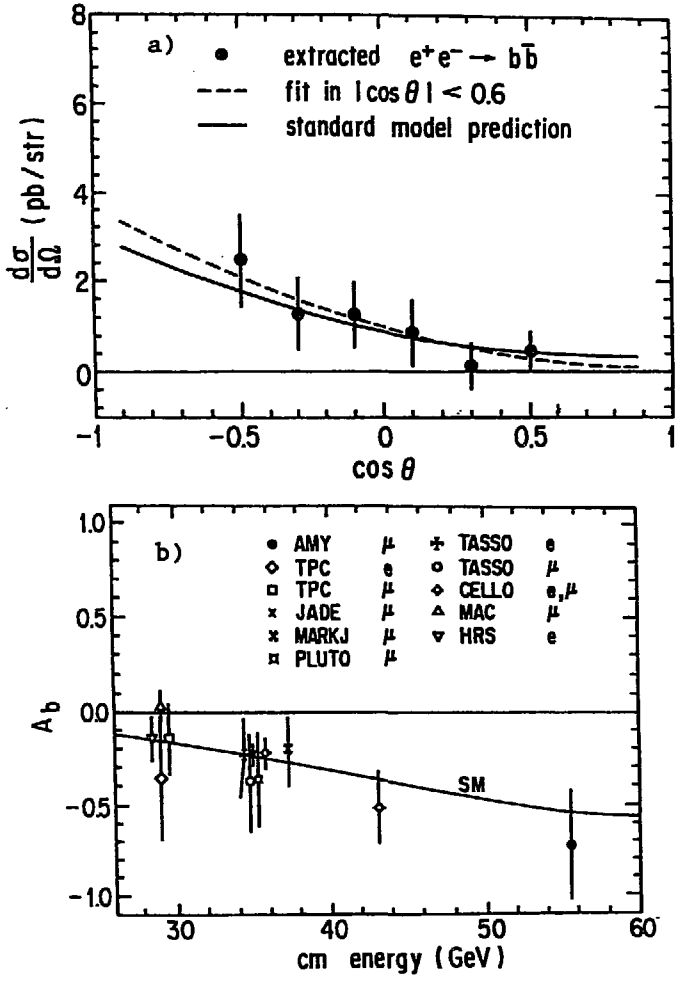

Figure 8. a) Differential cross section for $e^+e^- \to b\bar{b}$. The solid curve is the standard model prediction. The dashed curve is the result of the fit to the standard model. b) The measured forward-backward charge asymmetry for the $e^+e^- \to b\bar{b}$ at $\sqrt{s}$=55.2 GeV compared with the previous measurements as a function of c.m. energy. The solid curve is the standard model prediction.

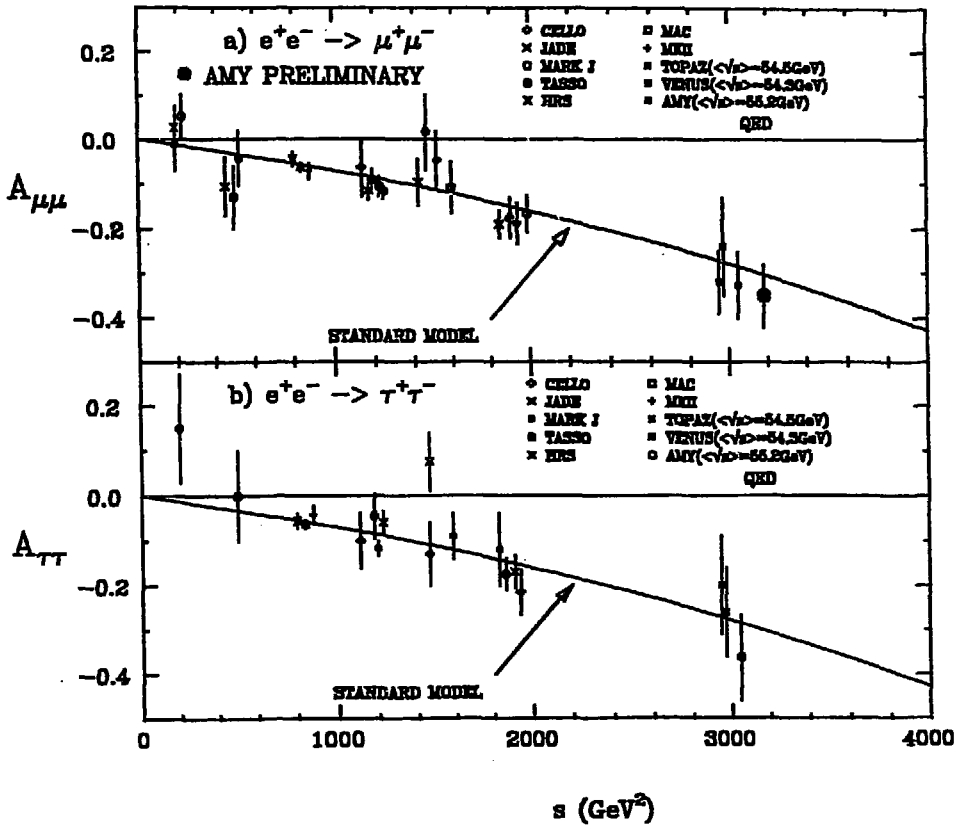

Figure 9. The forward-backward charge asymmetry for a) $e^+e^- \to \mu^+\mu^-$ and b) $e^+e^- \to \tau^+\tau^-$ as a function of the center of mass energy. The solid curve indicate the standard model prediction using M_Z=92 GeV, Γ_Z=2.5 GeV, and $\sin^2\theta_W$=0.230.

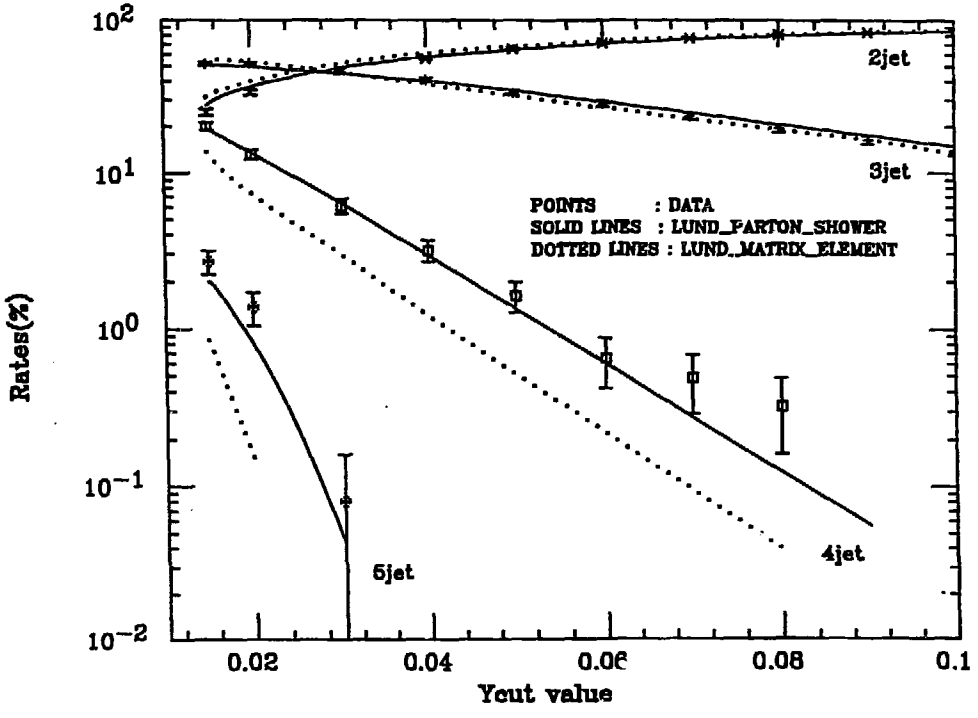

Figure 10. Jet multiplicity as a function of y_{cut}

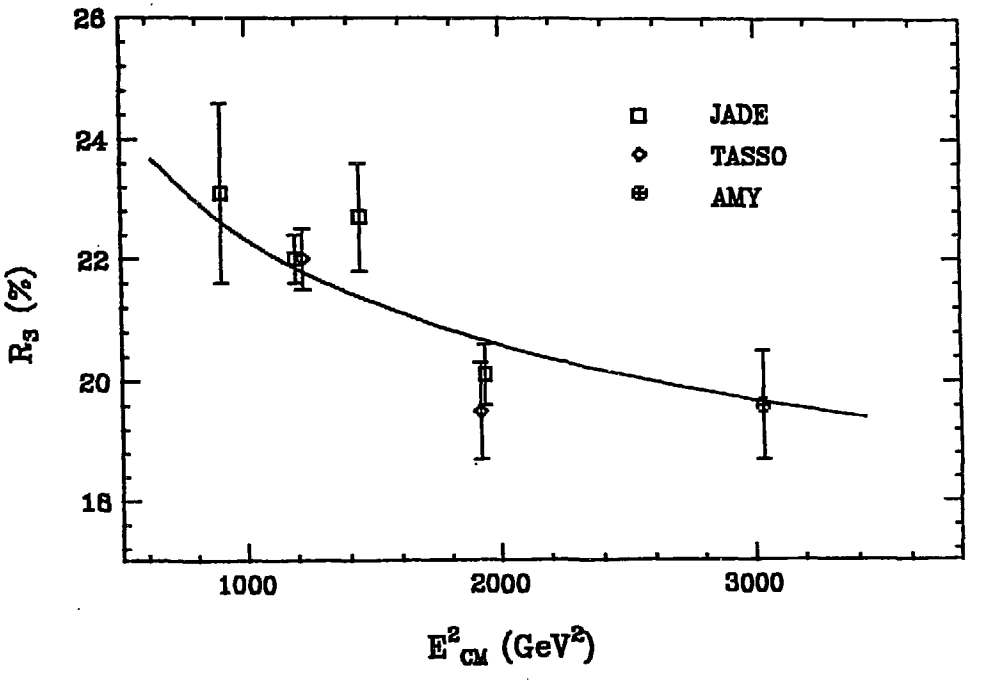

Figure 11. Measured values of R_3 with y_{cut} vs. E^2_{CM}. The solid line is based on a second order calculation by Kramer and Lampe.

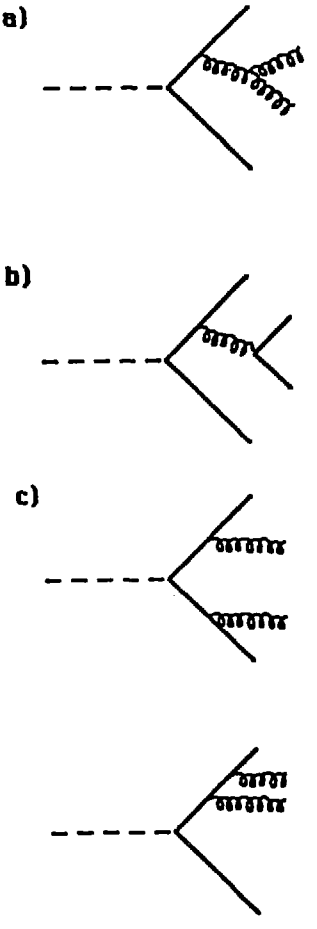

Figure 12. Diagrams that yield four-parton states.

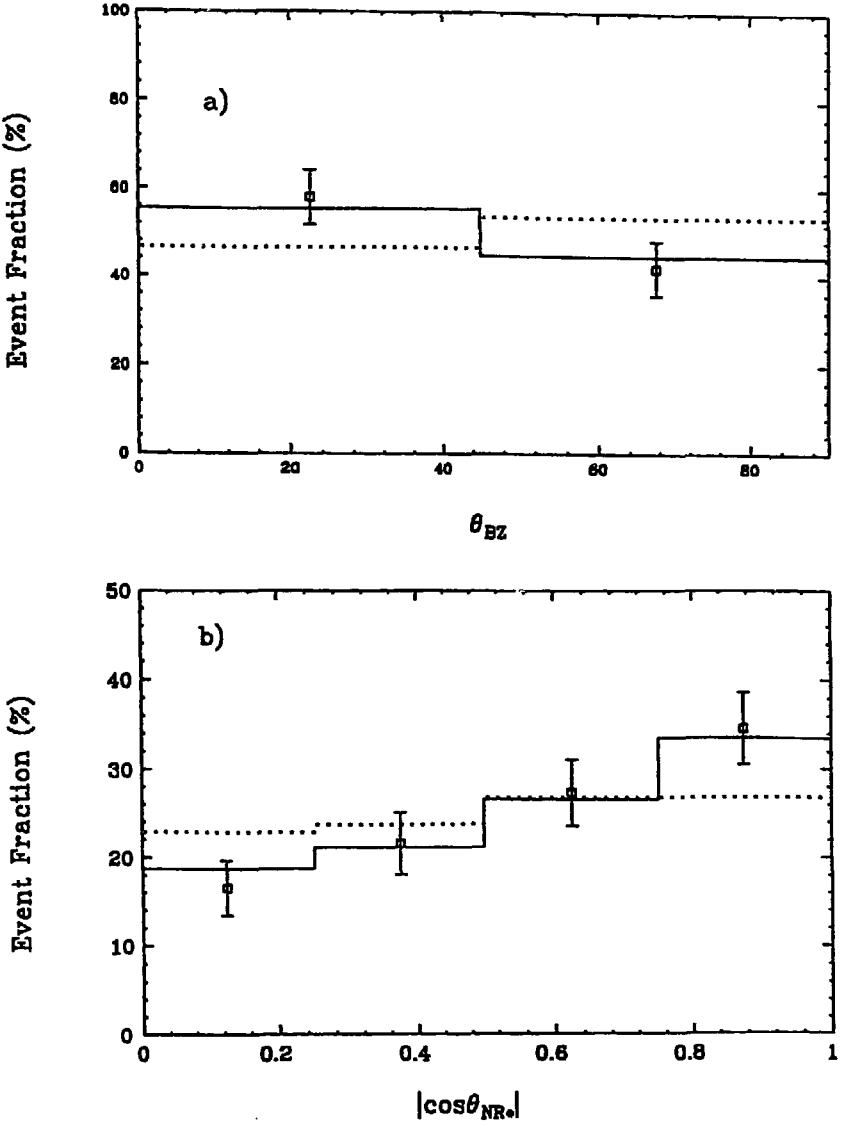

Figure 13. a) Distribution of θ_{BZ} and b) $|\cos\theta^*_{NR}|$ in four-jet events. Also shown, are the LUND 6.2 predictions for QCD (solid) and for the Abelian model (dashed).

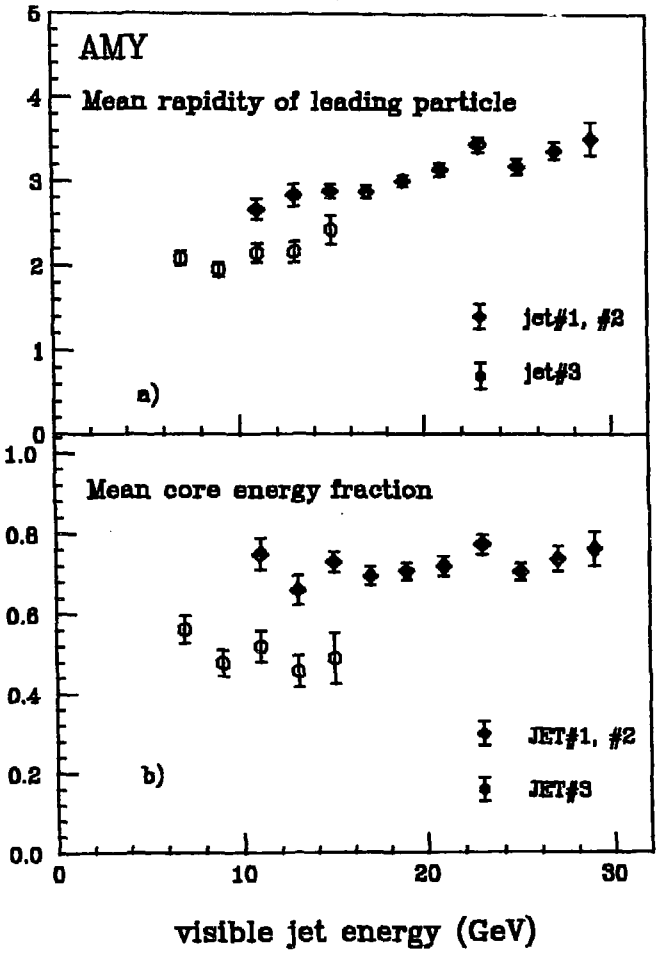

Figure 14. a) The mean rapidity of the leading particle in the jet, $< \eta^{lead} >$, and (b) the mean energy fraction in a cone of half angle $60°/\sqrt{E^{jet}_{vis}}$ coaxial with the jet axis, $< \xi^{cone} >$, as a function of the visible jet energy, E^{jet}_{vis}. The open points are for the gluon-enriched jet sample, the solid points for the quark-enriched sample.

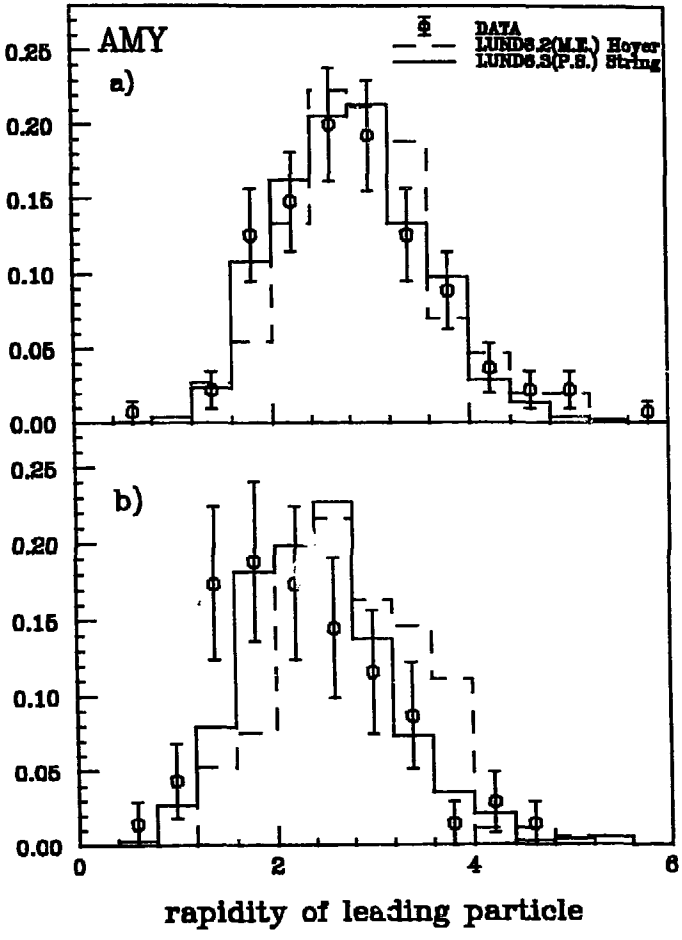

Figure 15. The distribution of leading particle rapidity, η^{lead}, for the a) quark-enriched and b) gluon-enriched jet samples. The dashed lines are the expectations from the $Q(\alpha_s^2)$ matrix element model with independent fragmentation. The solid lines are the expectations for the LLA model with string fragmentation.

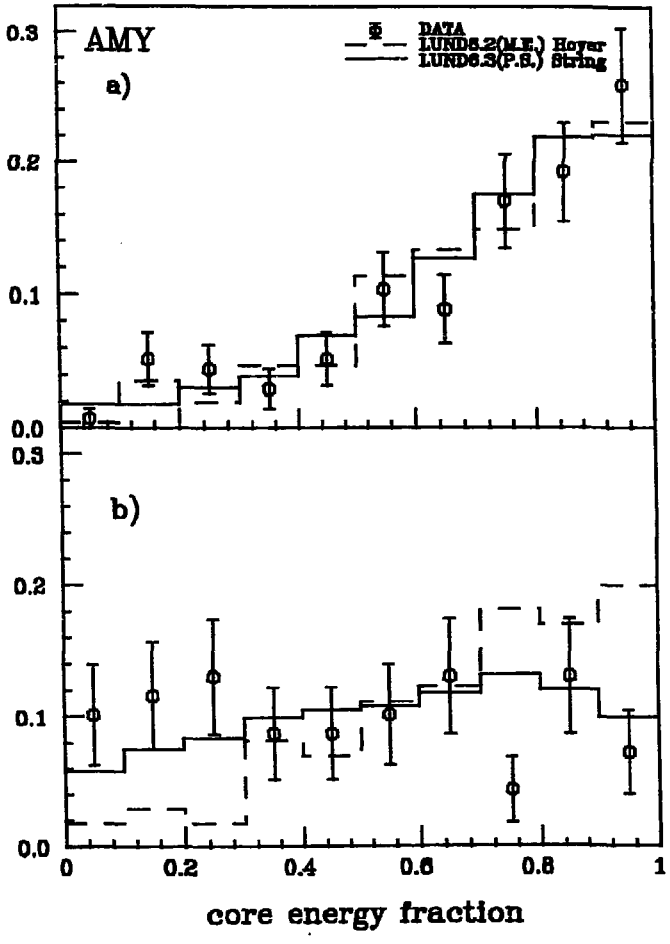

Figure 16. The distribution of the core energy fraction, ξ^{core}, for the a) quark-enriched and b) gluon-enriched jet samples. The dashed lines are the expectations from the $Q(\alpha_s^2)$ matrix element model with independent fragmentation. The solid lines are the expectations for the LLA model with string fragmentation.

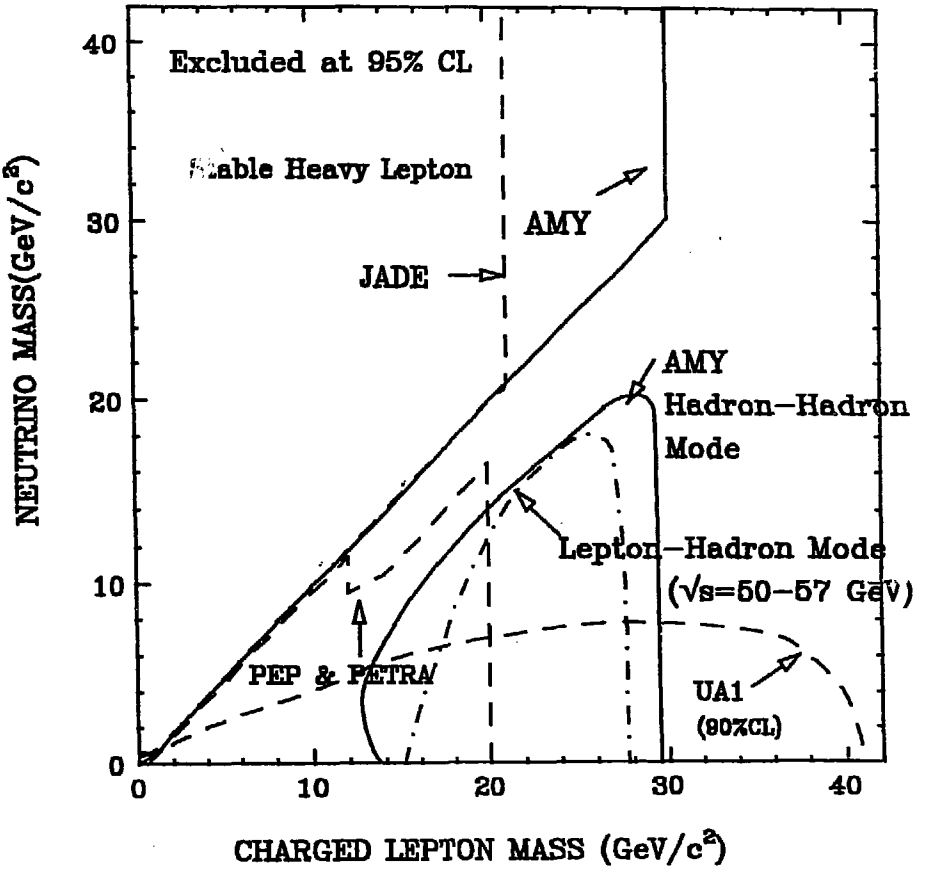

Figure 17. Region in the charged heavy lepton mass and neutrino mass plane excluded with 95% C.L. together with limits from other experiments.

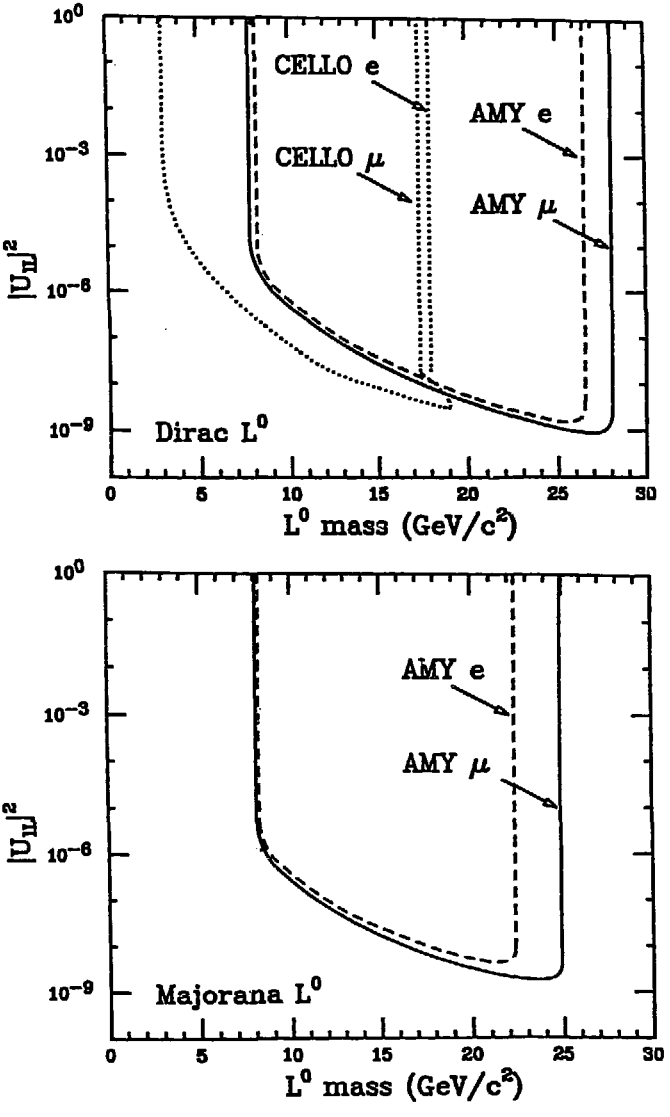

Figure 18. Mixing parameter $|U_{\ell L}|^2$ vs L^0 mass excluded regions at 95% C.L. for (a) Dirac, (b) Majorana neutrinos. Dashed [solid] line gives limits for dominant coupling to electrons [muons]. Dotted lines give CELLO limits.

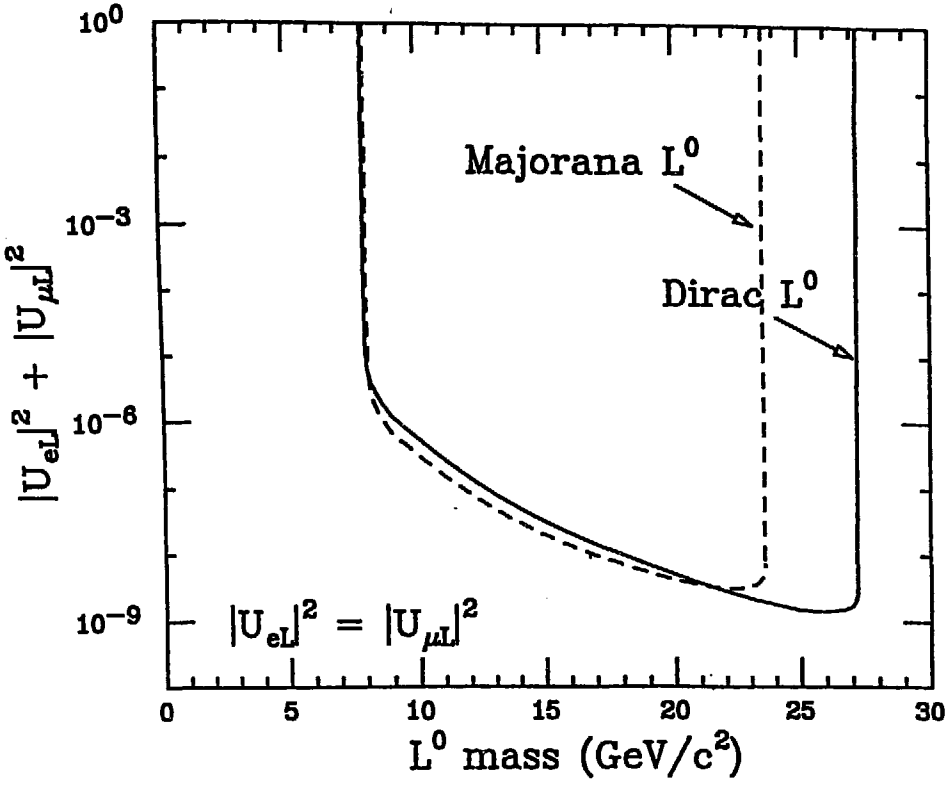

Figure 18. (c) Mixing parameter ($|U_{eL}|^2 + |U_{\mu L}|^2$) vs L^0 mass excluded regions at 95% C.L. for $Br(L^0 \to e f \bar{f}') = Br(L^0 \to \mu f \bar{f}') = 0.5$. Solid [dashed] line gives limits for Dirac [Majorana] neutrinos.

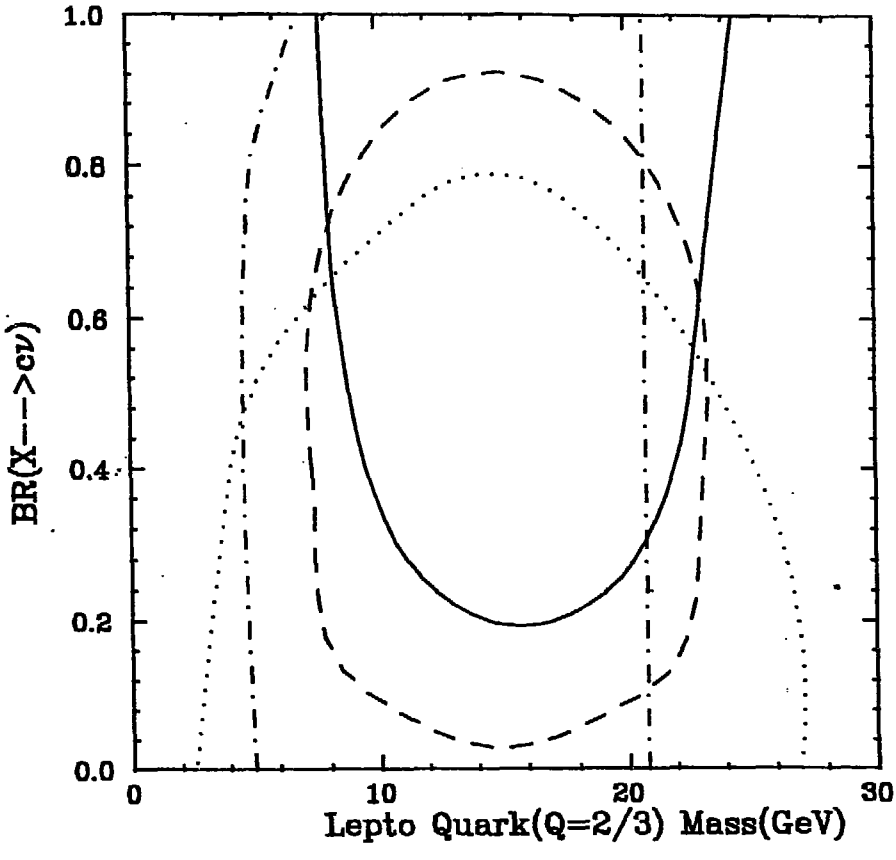

Figure 19. The 95% C.L. limit for leptoquark mass as a function of the branching fraction for $\chi \rightarrow c\bar{\nu}$. The solid, dashed, and doted lines represents acoplanar jets, isolated muons, and isolated dimuon selections, respectively. The dot-dashed line indicates the CELLO and JADE results.

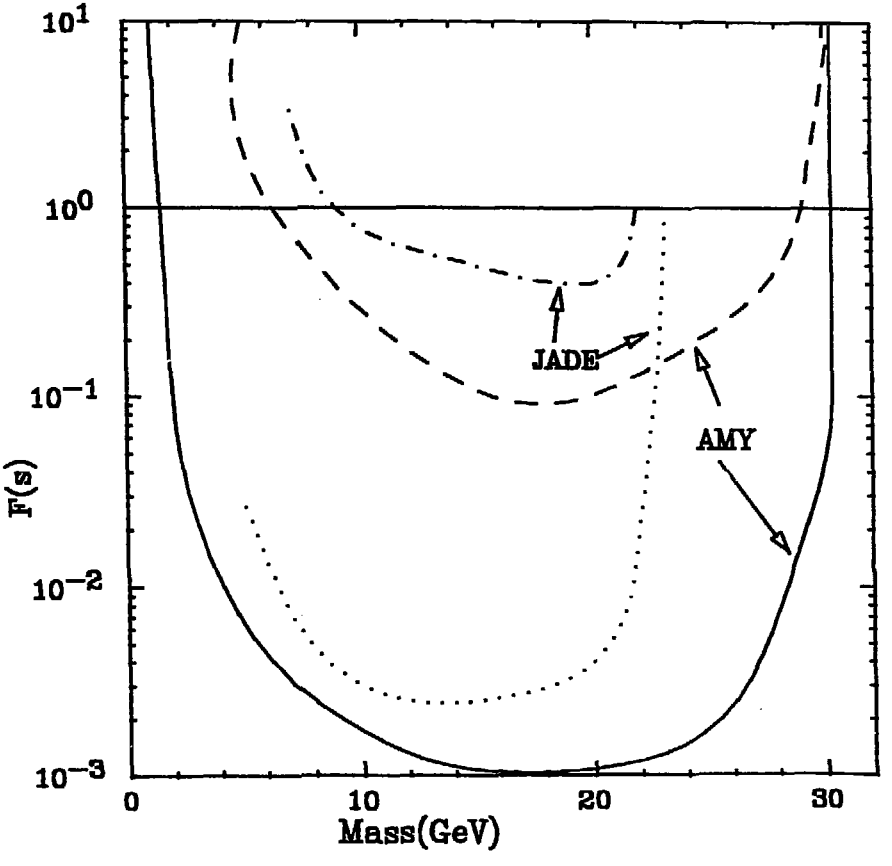

Figure 20. Limits on form factor F(s) for colored muon (solid line) and colored neutrino (dashed line) production. The JADE limits for colored muon (dotted line) and colored neutrino (dot-dashed line) are also shown.